**Proceedings of the Canadian Society for Mechanical Engineering International Congress**
**32nd Annual Conference of the Computational Fluid Dynamics Society of Canada**
**Canadian Society of Rheology Symposium**
**CSME/CFDSC/CSR 2025**
**May 25–28, 2025, Montréal, Québec, Canada**



# NUMERICAL ANALYSIS AND VALIDATION OF TURNING CIRCLE AND ZIG-ZAG MANEUVERS OF KRISO CONTAINER SHIP IN CALM SEA USING BODY FORCE METHOD

Adwaith Nath[1], Heather Peng[1], Wei Qiu[1],

[1]Advanced Marine Hydrodynamics Laboratory
Department of Ocean and Naval Architectural Engineering
Memorial University of Newfoundland
St John's, NL, Canada A1B 3X5
Email address: hpeng@mun.ca

Mar 27, 2025

***Abstract*—** Six-DoF Unsteady-Reynolds-Averaged-Navier-Stokes (URANS) CFD simulations are conducted using the body-force propeller based on the Hugh & Ordway model with Goldstein Optimum distribution to study and validate the maneuvering performance of KRISO container ship with the appended rudder in calm sea at Froude number $Fn = 0.26$. The $35^\circ$ port-side turning circle, $10^\circ$/ $10^\circ$ zig-zag starting to port, $20^\circ$/ $20^\circ$ zig-zag starting to port, and $20^\circ$/ $20^\circ$ zig-zag starting to starboard manoeuvrers suggested by the SIMMAN 2020 workshop are used for the validation study. Before the manoeuvrers are executed, the rudder is brought to the neutral position using a PID controller control such that the yaw angle is zero to mimic the suggested initial conditions. The two-phase incompressible simulations are solved using the STAR-CCM+ CFD software. The hull and rudder are meshed as separate overset grids to allow the 6DoF motion of the hull and the deflection of the rudder. The time histories of the predicted ship trajectory, motion, orientation, and velocities are illustrated and validated against the experiments, along with a comparison of maneuvering-specific parameters. The comparisons show that the use of the body-force propeller model is an efficient and effective method for ship maneuvering simulations

***Keywords-component*—Turning Circle; Zig-Zag; CFD; Controllers; KCS**

## I. INTRODUCTION

Assessing the maneuvering characteristics of ships is increasingly important in maritime operations to ensure safe and efficient operations. Accurate assessment of the maneuverability of the ship requires specialized facilities or computational resources to ascertain that the intended performance is achieved. The increased computational performance over the years, the ease of availability of these resources, and improvements in RANS-based models' accuracy have led to the increasing use of RANS simulations in assessing ship characteristics and performance. In the past decade, breakthroughs in overset technology have proven to be a crucial link in studying complex maneuvers. Several studies have been conducted to validate and assess the maneuvering performance of ships using fully discretized data, providing valuable information regarding the associated flow particulars and complex interactions involved. These simulations require a lot of computational resources due to the requirement of a meshed propeller and a small time step ($1^\circ - 2^\circ$ propeller rotation per time step), thus restricting the commercial viability of the method. Mathematical models provide a good alternative to fully discretized propellers but are highly sensitive to the model inputs.

This paper focuses on assessing the performance of the Hugh & Ordway model with Goldstein Optimum distribution body-force propeller in maneuvering simulations. Continuing on the work by [6], the cases studied are maneuvers of KCS hull in deep and calm water at Froude Number $Fn = 0.26$ suggested in SIMMAN 2020 workshop [9] which are $35^\circ$ port-side turning circle, $10^\circ$/ $10^\circ$ zig-zag starting to port, $20^\circ$/ $20^\circ$ zig-zag starting to port, and $20^\circ$/ $20^\circ$ zig-zag starting to starboard. Prior to the execution of the maneuvers, two simulations are conducted using a PI controller and PID yaw controller to

mimic the recommended initial conditions. Descriptions of the numerical method, body-force model, controllers, and procedures followed for the simulations are reported. Finally, the maneuvering simulation results are validated against MARIN experiments.

## II. Numerical Modelling

### A. Governing equations

The governing RANS equations for viscous flow with the assumption for incompressibility are:

$$\begin{aligned} \frac{\partial \rho}{\partial t} + \nabla \cdot (\rho \overline{\mathbf{v}}) &= 0 \\ \frac{\partial \rho \overline{\mathbf{v}}}{\partial t} + \nabla \cdot (\rho \overline{\mathbf{v}} \otimes \overline{\mathbf{v}}) &= -\nabla \cdot \overline{P}\mathbf{I} + \nabla \cdot \mathbf{T} + \mathbf{f_b} \end{aligned} \tag{1}$$

where $\overline{\mathbf{u}}$ is the mean velocity vector, $\rho$ is the density, $\overline{P}$ is the mean pressure, $\mathbf{I}$ is the Identity Matrix, $\mathbf{T}$ is the Reynolds stress tensor and $\mathbf{f_b}$ is the resultant of the body forces.

Solving the RANS equation requires using turbulence models to close the problem. In this paper, the $k-\omega$ SST model is used per the best practice settings recommended by [1] for two-phase marine simulations. The $k-\omega$ SST proposed by [2] is based on the Boussinesq Hypothesis which equates $\mathbf{T}$ to mean velocity gradients and eddy viscosity $\mu_\mathbf{T}$ as:

$$\mathbf{T} = \mu_\mathbf{T} \left[ \nabla \overline{\mathbf{v}} + (\overline{\mathbf{v}})^T \right] - \frac{2}{3} \rho k \mathbf{I} \tag{2}$$

The $k-\omega$ $SST$ switches between the $k-\omega$ model near walls and the $k-\epsilon$ model in the free stream to improve predictions in adverse pressure gradients and separating flow. The two-phase simulations used the Volume-of-Fluid (VoF) model and the High-Resolution-Interface-Capturing Method (assuming immiscibility of fluids) implemented in StarCCM+ CFD software to capture the sharp interface between the two fluids.

### B. Body-force propeller model

The body-force propeller method uses a distribution of momentum sources over a cylindrical virtual disc to emulate the propeller thrust and torque. The implementation of the body-force propeller model in StarCCM+ follows the non-iterative calculation of [3], the circulation distribution of [4] with optimum type from [5].

The axial and radial components of the body force moment source terms using the Goldstein optimum distribution are given by:

$$\begin{aligned} f_{bx} &= A_x r^* \sqrt{1 - r^*} \\ f_{b\theta} &= A_\theta \frac{r^* \sqrt{1 - r^*}}{r^*(1 - r'_h) + r'_h} \end{aligned} \tag{3}$$

where

$$r^* = \frac{r' - r'_h}{1 - r'_h}; \quad r'_h = \frac{R_H}{R_P}; \quad r' = \frac{r}{R_P} \tag{4}$$

and constant $A_x$ and $A_\theta$ are define as:

$$\begin{aligned} A_x &= \frac{105}{8} \frac{T}{\pi \Delta (3R_H + 4R_P)(R_P - R_H)} \\ A_\theta &= \frac{105}{8} \frac{Q}{\pi \Delta R_P (3R_H + 4R_P)(R_P - R_H)} \end{aligned} \tag{5}$$

Here $r$ is the radial coordinate, $R_H$ is the hub radius, $R_P$ is the propeller tip radius, $T$ is the thrust, $Q$ is the torque, and $\Delta$ is the virtual disk thickness. The thrust and torque values are calculated using the interpolated thrust and torque coefficients from the open-water performance table at the advance coefficient ($J$) corresponding to the current average velocity at the inflow plane. The open-water performance table used for the actuator disk is from open-water propeller tests of the same model scale by [6].

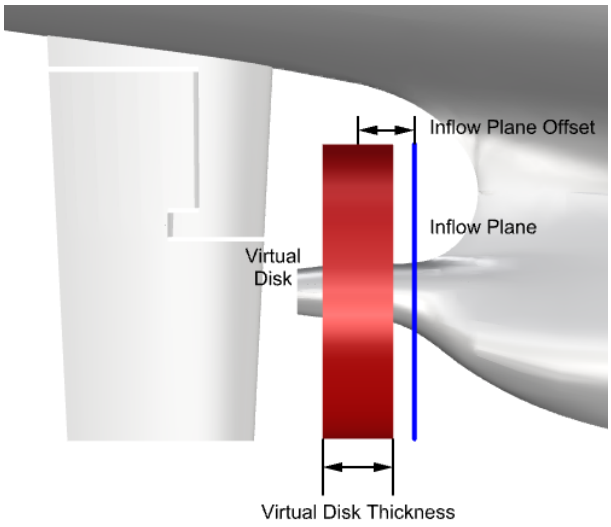


Figure. 1: Virtual Disk parameters

The parameters of the virtual disk body force model (Fig:1) follow the best practice recommendations by [1]. Accordingly, the thickness of the virtual and the offset of the inflow plane are $0.24D_P$ and $0.20D_P$, respectively, where $D_P$ is the propeller diameter. The body-force model enables a higher time step than a fully discretized rotating propeller, significantly reducing computational cost. The time step used for all the simulations is $0.1s$.

### C. Controllers

*1) Propeller RPS controller:* To calculate the revolutions-per-second(rps) of the propeller at the self-propulsion point for the velocity corresponding to the target $Fn$, a Proportional-Integral (PI) controller is used. The PI controller uses the following formulation:

$$\begin{aligned} n &= max\left( n_i \left( Pe_F + I \int_0^t e_F \, dt \right), 1. \right) \\ e_F &= v_t - v_x \end{aligned} \tag{6}$$

Here, $n$ is the predicted rps, $n_i = 35.0$ is the initial rps estimate, $v_t$ and $v_x$ are the targets and current X velocity of the ship, respectively, $P = 1.5$ is the proportional constant and $I = 1.0$ is the integral constant. The predicted rps is not allowed to go below one rps to avoid negative rps predictions, which could occur at the start of the simulation when the ship is stationary.

*2) Yaw Controller:* To calculate the neutral rudder angle, a proportional-integral-differential (PID) yaw controller is used to control the rudder angle so that the yaw angle of the ship is zero. The definition of the yaw controller is as follows:

$$\delta = Pe_F + I\int_0^t e_F\ dt + D\frac{de_F}{dt} \qquad (7)$$
$$e_F = \psi_t - \psi$$

Here, $\delta$ is the predicted rudder angle, $\psi_t = 0$ and $\psi$ are the target and current yaw angle of the ship, respectively, $P = 2.4$ is the proportional constant, $I = 0.5$ is the integral constant and $D = 4$ is the differential constant.

## III. Geometry and Coordinate System

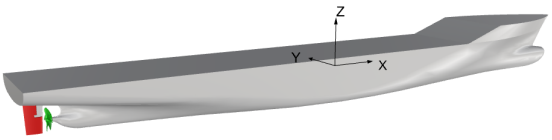


Figure. 2: KCS hull, rudder and propeller geometry

The KCS hull with appended rudder and propeller with a scale ratio $\gamma = 37.89$ is shown in the Fig. 2. The model's main particulars are tabulated in Table I. A right-handed coordinate system is used with x axis towards the bow, y axis toward port and the origin located at the intersection of the symmetry plane of the ship, the design water-plane and the midship plane.

TABLE. I: Main Particulars of Geometry

| | Unit | Full Scale | Model Scale |
|---|---|---|---|
| **Scale** | - | 1 | 37.89 |
| **Lpp** | $(m)$ | 230 | 6.0702 |
| **Lwl** | $(m)$ | 232.5 | 6.1355 |
| **Bwl** | $(m)$ | 32.2 | 0.8498 |
| **Depth** | $(m)$ | 19 | 0.5015 |
| **Draft** | $(m)$ | 10.8 | 0.285 |
| **Displacement** | $(m^3)$ | 52057 | 0.957 |
| **LCG from AP** | $(m)$ | 111.6 | 2.945 |
| **GM** | $(m)$ | 0.6 | 0.016 |
| $\boldsymbol{i_{xx}/B}$ | - | 0.4 | 0.4 |
| $\boldsymbol{i_{yy}/Lpp}$ | - | 0.258 | 0.25 |
| $\boldsymbol{i_{zz}/Lpp}$ | - | 0.258 | 0.25 |

## IV. Computational Domain And Mesh Details

The computational domain is comprised of a background domain with the hull domain and rudder domain as oversets to facilitate the relative motion between hull & background and the rudder & hull(Fig:3 and Fig:4). The background extends $2L_{pp}$ forward of the bow, $3L_{pp}$ aft of the transom, $1.65L_{pp}$ below the free surface, $1L_{pp}$ above the free surface and $2L_{pp}$ on either side of the symmetry plane of the hull.

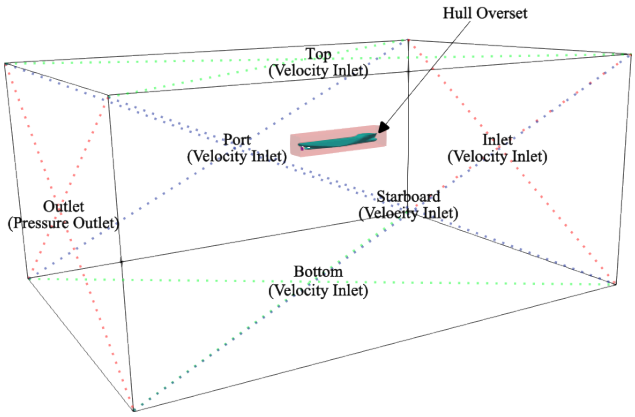


Figure. 3: Background and Hull Overset Domains

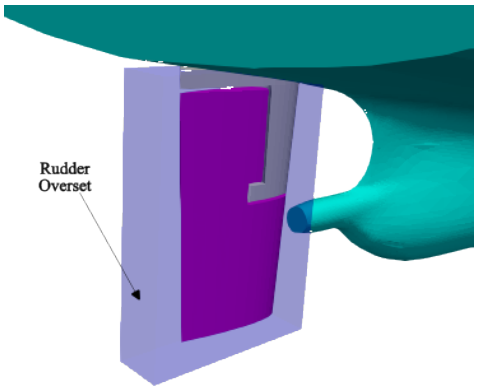


Figure. 4: Rudder Overset Domains

The computation grids are generated using the meshing utility of the StarCCM+ CFD software. Following the recommendations by [1], the hull is refined such that the number of cells along the length of the hull $L_{pp}/\Delta x = 775$. Prism layers are inserted along the wall surfaces to achieve a target $y^+ = 60$ (Fig:5). Cells are refined along the z direction anisotropically close to the design waterline to ensure a good resolution of the free surface while reducing the computational effort.

Cells along the boundaries of overset grids and corresponding

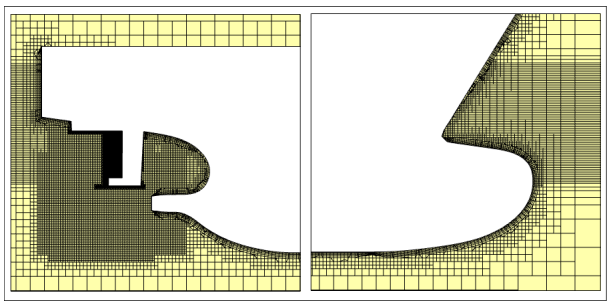

Figure. 5: Hull Grid - Stern and Bow

overlap regions are refined to maintain similar cell sizes

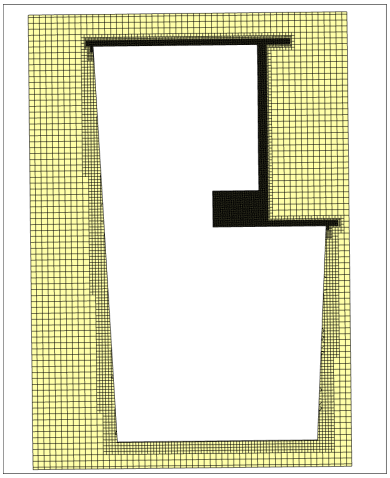

Figure. 6: Rudder Grid

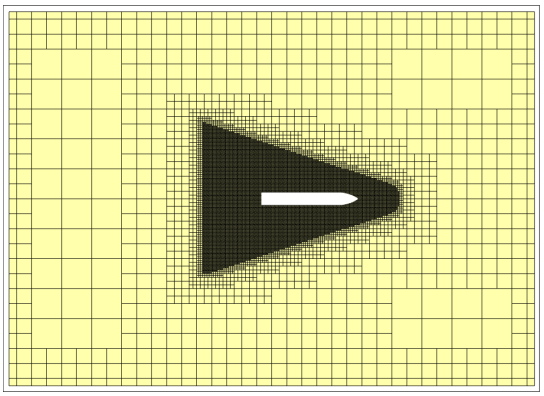

Figure. 7: Kelvin Wake Refinement

between domains for proper overset interpolations between domains. Special care is taken in the case of the gap between the rudder-stock and the rudder by inserting very fine cells in the gap and along the rotational trajectory of the rudder to ensure sufficient cells are present between the rudder-stock and the rudder to be marked for interpolation.(Fig: 6). Cells are refined along the x and y direction along the free surface close to the hull (Fig:7) to capture the kelvin wake of the ship. The final computational mesh constitutes a cumulative cell count of 9.8 M, with the background, hull, and rudder domain meshes comprised of 1.8 M, 6.5 M, and 1.5 M cells, respectively.

## V. Simulation Methodology

Prior to the execution of the maneuver, as per instructions on the SIMMAN KCS deep water and trajectories [9], the propeller rps is to be fixed at the self-propulsion point of the ship, and the rudder angle should be oriented such that the yaw of the ship $\psi = 0$. These initial conditions were achieved using the self-propulsion and rudder neutral simulations. In the self-propulsion simulation, the propeller PI controller obtains the propeller rps at self-propulsion at $Fn = 0.26$ with the ship free to surge, heave, and pitch. For the neutral rudder simulation, with the propeller fixed at the rps obtained from the self-propulsion simulation and the ship allowed to move in all 6 DoF, the rudder angle is controlled using the yaw controller such that the yaw of the ship is at a steady value of $\psi = 0$ thus matching the required initial conditions of the experiments. Finally, the controls specific to each maneuver are then executed. For the $35^\circ$ port-side turning circle simulation, the rudder is rotated from the neutral position to the $35^\circ$ port at a fixed rudder angle rate, and the simulation is performed till the ship completes a circle. For zig-zag $10^\circ/10^\circ$ port-side simulation, the rudder is rotated from the neutral rudder angle to $10^\circ$ port till the $\psi = 10^\circ$. Then the rudder is rotated to $10^\circ$ starboard till the $\psi = -10^\circ$ and the procedure is continued till three executes are completed. Similar procedures are followed for zig-zag $20^\circ/20^\circ$ port-side and zig-zag $20^\circ/20^\circ$ starboard-side simulations.

TABLE. II: Initial Conditions

| | CFD | EFD |
|---|---|---|
| **Propeller Rotation Rate (rps)** | 12.351 | 11.496 |
| **Rudder Angle (degree)** | -0.427 | -0.020 |

TABLE. III: Turning Circle $35^\circ$ port Validation

| | CFD | EFD | E%D |
|---|---|---|---|
| **Tactical Diameter $y_{O180}$ (m)** | 2.476 | 2.640 | -6.22 |
| **Advance $x_{O90}$ (m)** | 2.873 | 2.934 | 2.08 |
| **Transfer $y_{O90}$ (m)** | 1.016 | 1.085 | -6.44 |
| **Steady Turning Radius $R_C$ (m)** | 1.102 | 1.221 | -9.74 |
| **$u$ (m/s)** | 0.751 | 0.814 | -7.73 |
| **$v$ (m/s)** | 0.308 | 0.271 | 13.73 |

## VI. Results and Discussion

As mentioned in the previous section, the self-propulsion and neutral rudder simulations were conducted to set the initial conditions according to [9]. The resulting initial condition shows slight deviations in the propeller rps and the rudder angle compared to the experiments (Table: II). The rps for the self-propulsion point using the Actuator Disk model was obtained as 12.35 was slightly over-predicted compared to the 11.50 rps obtained from the experiment. This deviation results from the variations in the model used by CFD and MARIN as reported by [6], leading to deviations in the KT KQ performance curves. As the experiments did not use a yaw controller to enforce the yaw of the vessel to zero, deviations were also observed in the initial rudder angles for maneuvers compared to CFD. However, the effects of the slight variations in the initial conditions are concluded to have negligible effects, and the values of the deviations are small, as the results of the maneuvering simulations show good comparison with the experiments.

The ITTC parametric comparisons of the turning circle maneuver (Table III) show good agreement with experimental observations. Deviations are within 10% of the experiments for distance-related parameters. Higher deviations are observed in velocity parameters $u$ and $v$, mainly associated

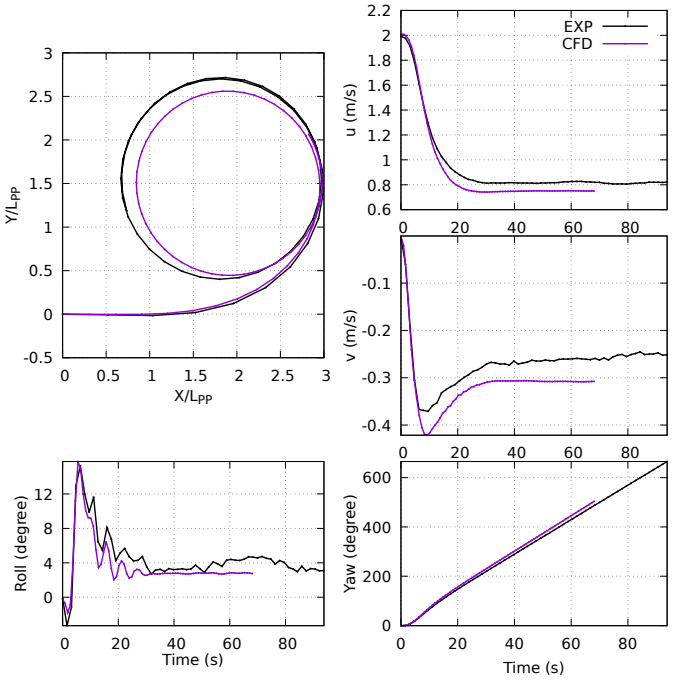


(a) Turning Circle 35° - Trajectory, $u$, $v$ and yaw

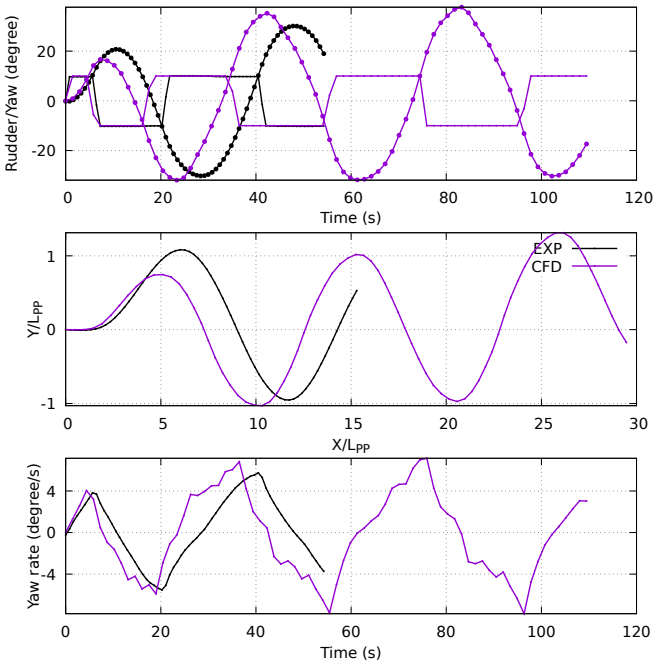


(b) Zig-Zag 10°/10° port - Yaw, rudder, trajectory, and yaw rate

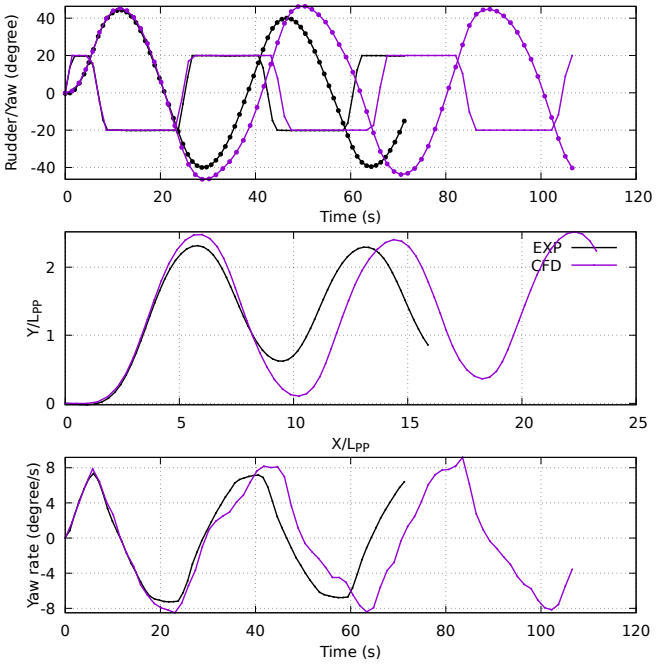


(c) Zig-Zag 20°/20° port - Yaw, rudder, trajectory and yaw rate

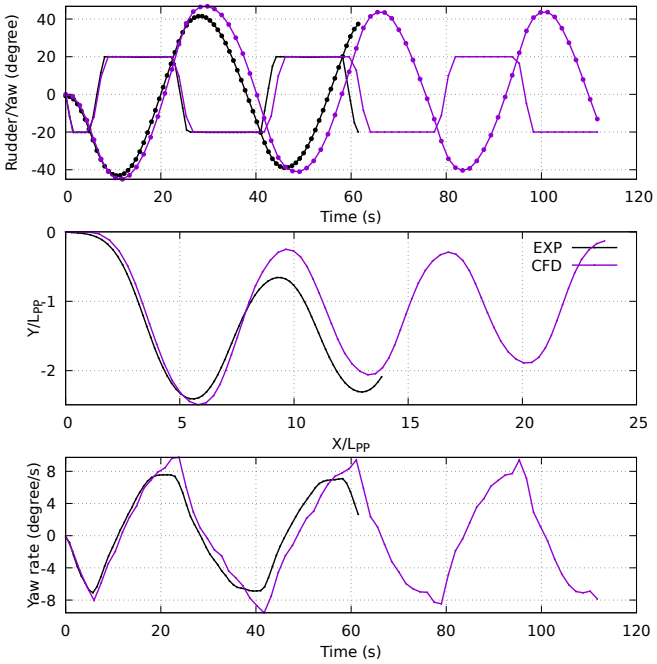


(d) Zig-Zag 20°/20° starboard - Yaw, rudder, trajectory, and yaw rate

Figure. 8: Manoeuvring Simulations - Position, Orientation, and Velocities

TABLE. IV: Zig-Zag Validations

| | **10°/10° port** | | | **20°/20° port** | | | **20°/20° stbd** | | |
|---|---|---|---|---|---|---|---|---|---|
| | **CFD** | **EFD** | **E%D** | **CFD** | **EFD** | **E%D** | **CFD** | **EFD** | **E%D** |
| **Initial Turning Time $t_a$ (s)** | 4.750 | 5.640 | -15.78 | 5.470 | 5.500 | -0.55 | 5.400 | 5.140 | 5.06 |
| **Overtshoot $1^{st}$ execute (degree)** | 6.728 | 10.761 | -37.48 | 25.387 | 24.398 | 4.05 | 25.156 | 23.219 | 8.34 |
| **Heading Change Time $1^{st}$ $t_s$ execute(s)** | 2.890 | 5.040 | -42.66 | 6.080 | 6.060 | 0.33 | 6.170 | 5.830 | 5.83 |
| **Overshoot $2^{nd}$ execute (degree)** | 21.954 | 20.228 | 8.53 | 26.504 | 20.044 | 32.23 | 26.816 | 21.583 | 24.24 |
| **Heading Change Time $2^{nd}$ execute $t_b$(s)** | 7.100 | 8.260 | -14.04 | 6.050 | 5.320 | 13.72 | 6.270 | 5.600 | 11.96 |
| **Reach $t_A$ (s)** | 14.430 | 18.320 | -21.23 | 20.890 | 20.900 | -0.05 | 20.800 | 20.000 | 4.00 |
| **Time Cycle $T$ (s)** | 32.940 | 38.680 | -14.84 | 41.320 | 38.320 | 7.83 | 40.180 | 38.050 | 5.60 |

with different rps used in the experiment and CFD and also the ability of the actuator disk used in CFD to model the side forces produced by the propeller while in the oblique non-uniform wake of the ship. Another major factor is associated with the overset interpolation between the background and the mesh. The cells at the boundaries of the hull domain are anisotropically refined and are misaligned due to high roll angles associated with the maneuver, leading to less accurate marking and interpolation between donor and acceptor cells. The trajectory plot (Fig.8a) shows similar predictions for CFD and EFD with a smaller diameter of the turning circle predicted by CFD due to the higher $v$ velocity and lower $u$ velocity.

The validations of the zig-zag simulations are tabulated in Table: IV and the yaw, rudder, trajectory, and yaw rate plots are shown in Fig:8. In cases of the 20°/20° port and starboard maneuvers show good agreement for $1^{st}$ execute with deviations below 5% for port side maneuver and 9% for starboard side maneuver. But Higher variations are observed for $2^{nd}$ execute specifically for the overshoot, with a deviation of 33.23% and 24.24% for port and starboard side maneuver, respectively. For the 10°/10° port, results show much higher variations in the $1^{st}$ execute ranging up to 42.66% but reduces to 21.23% in the $2^{nd}$ execute.

A cause for the deviations is due to faults in the experiments where the target rudder angle is not achieved (Figure: 8b, Figure: 8c and Figure: 8d)and the trends also correspond to this problem. In the zig-zag 10°/10° port, where it is more prominent, the rudder angle is set to 9.7° in the $1^{st}$ execute, leading to a larger overshoot and in the $2^{nd}$ execute the rudder angle is set to 10.2°7 leading to a compensating effect and a lower deviation in the corresponding overshoot value in comparison with CFD. A similar case occurs in zig-zag 20°/20° port maneuver; the rudder is set to 19.7° in the $1^{st}$ and 20.2° in the $2^{nd}$ execute. An opposite case is observed in the zig-zag 20°/20° starboard maneuver where the rudder is set to 20.2° in the $1^{st}$ and 19.7° in the $2^{nd}$ execute. The effects of the overset interpolation at the boundaries are also the reason for the deviations. This effect of the overset interpolation can be observed in Figure: 9 when the roll of the vessel is high (Figure:9c) there are several artifacts on the free surface due to the poor quality of interpolation at the boundaries between the background and the hull domains as the roll reduces (Figure:9b) the quality of the overset interpolation is improved and when roll is close to zero, that is, when the meshes align, we can see no artifacts and observed a free surface with good resolution(Figure:9a). The effect of this problem is less significant in zig-zag maneuvers due to the transient nature of roll associated with the maneuver, but it is more significant in the turning circle as the mesh is constantly at a high roll angle, leading to misalignment between the cells in the steady phase of the maneuver. Methods to mitigate the overset interpolation at the boundaries and free-surface include Adaptive Grid Refinement (AGR) or isotropically refined free surface cells in the hull domain, both leading to a significant increase in the computational effort.

## VII. Conclusion

The turning circle and zig-zag simulations of the model-scale KCS hull appended with rudder at $Fn = 0.26$ are studied using the body-force actuator disk model using the StarCCM+ CFD software and validated against experiments from MARIN.

The initial conditions of rps and yaw of the ship are matched with the case setup mentioned in SIMMAN "KCS deep water waves and trajectories" [9] by performing a 3 DoF simulation using a PI propeller rps controller to obtain rps at the self-propulsion point and a 6 DoF simulation using a PID yaw controller to set the rudder at the neutral rudder angle position. Slight variations were observed in CFD initial conditions compared to experiments but the effect of the variations was negligible on the results of the maneuvers.

Comparisons of the CFD maneuvering simulations against experiments were performed using ITTC-recommended parameters and generally showed good predictions. The 35° post-side turning circle simulations generally show good comparison with distance-related parameters within 10% and velocities within 16% . The parametric comparisons of the zig-zag simulations for 20°/20° port and starboard zig-zag simulations show deviations less than 10% for parameters associated with the $1^{st}$ execute but deviations up to 33% for parameters associated with $2^{nd}$ execute. The deviations in the 10°/10° port zig-zag simulations were higher variations of up to 43%. The main reason for deviations in zig-zag simulations arises from the experimental errors. Other sources of deviations of the maneuvering simulations include the

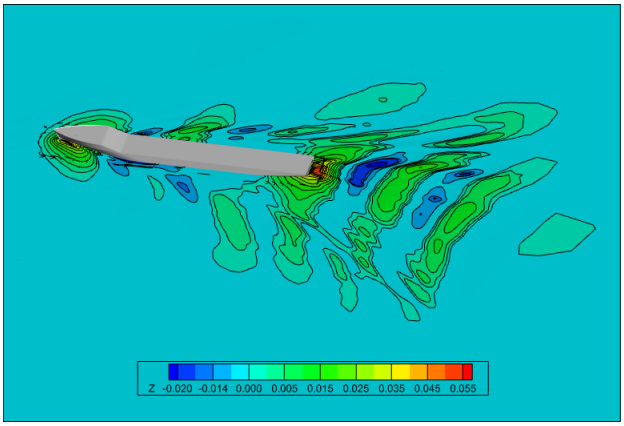


(a) Zig-Zag 10°/10° port

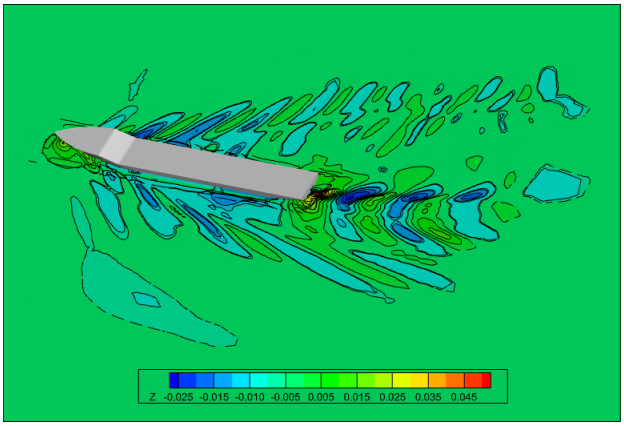


(b) Zig-Zag 20°/20° port

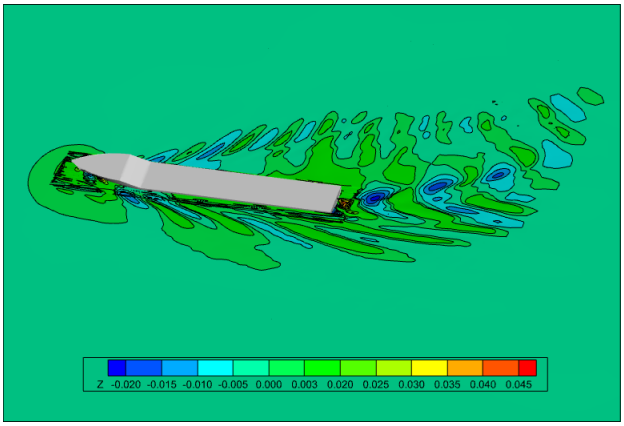


(c) Zig-Zag 20°/20° starboard

Figure. 9: Free Surface

imprecise modeling of the forces by the actuator disk model in non-uniform oblique flows, leading to differences in velocities and inaccurate overset interpolation at the boundaries between the hull and the background domain, specifically at the free surface. The study shows that using the body-force model based on the Hugh & Ordway model with Goldstein optimum distribution is efficient for predicting the turning circle and zig-zag maneuvers with reasonable accuracy. Future work includes providing a comprehensive overview of the accuracy of other propeller models in literature against fully discretized rotating propellers and experiments for maneuvering simulations for calm water and waves.

## REFERENCES


[1] Jin, Shanqin and Peng, Heather and Qiu, Wei and Oldfield, Chad and Stockdill, Barton, "Best modeling practice for self-propulsion simulation of ship model in calm water", Physics of Fluids, 2023

[2] F.R. Menter, M. Kuntz, and R. Langtry, "Ten years of industrial experience with the SST turbulence model", In Proceedings of the fourth international symposium on turbulence, heat and mass transfer, pages 625–632, Antalya, Turkey, 2003. Begell House

[3] Stern, F and Kim, HT and Patel, VC and Chen, HC, "A viscous-flow approach to the computation of propeller-hull interaction", Journal of Ship Research, pages 246–262, 1988

[4] Hough, G. and Ordway, D., "The generalized actuator disc", Technical Report TAR-TR6401, 1964. Therm Advanced Research, Inc.

[5] Goldstein, Sydney, "On the vortex theory of screw propellers", Proceedings of the Royal Society of London. Series A, Containing Papers of a Mathematical and Physical Character, vol 123, pages 440–46, 1929. The Royal Society London

[6] Nath, Adwaith and Peng, Heather and Qiu, Wei (26–29 May 2024), "RANS simulation to determine the self-propulsion point of the Kriso Container Ship using PI Controller", Presented at the 32nd Annual Conference of the CFD Society of Canada,Toronto, Canada

[7] Deng, Ganbo and Queutey, Patrick and Wackers, Jeroen and Visonneau, Michel and Guilmineau, Emmanuel and Leroyer, Alban, "Assessment of ship maneuvering simulation with different propeller models", Journal of Hydrodynamics, vol 34, pages 422–433, 2022, Springer

[8] Procedures, ITTC Recommended, "Guideline on Use of RANS Tools for Manoeuvring Prediction", Proceedings of 26rd ITTC, 2011

[9] SIMMAN2020, "Workshop on Verification and Validation of Ship Manoeuvring Simulation Methods", 2020. https://www.simman2020.kr